Proceedings of the ASME 2010 3rd Joint US-European Fluids Engineering Summer Meeting and 8th International Conference on Nanochannels, Microchannels, and Minichannels
FEDSM-ICNMM2010
August 1-5, 2010, Montreal, Canada

FEDSM-ICNMM2010-31113

EXPERIMENTAL MEASUREMENT OF MIXING LENGTHS OF CONVERGING PARTICULATE FLOWS IN MICROCHANNELS

Michael Nadler
Graduate Student
Mechanical Engineering Program
School of Engineering
University of Vermont
Burlington, VT 05405 USA

Darren L. Hitt*
Associate Professor
Mechanical Engineering Program
School of Engineering
University of Vermont
Burlington, VT 05405 USA

ABSTRACT

Laminar flow mixing remains an active area of research within the microfluidics community. Traditional mixing methods often rely upon turbulent flow for mixing which is generally not present on the micro-scale and so alternative approaches must be sought. In this work we investigate the potential for enhanced laminar mixing due to the addition of inert particles, of varying size and concentration, to converging flows of miscible fluids at a 3-way microchannel 'Y junction. One inlet fluid is fluorescently-labeled to enable imaging of the converging fluid interface downstream of the junction. Using the techniques of fluorescent microscopic imaging and digital image analysis, the degree of mixing is quantified for varying flow states by the measurement of dye concentration (intensity) profiles at downstream locations. It is found that the addition of particulates to the flow does not noticeably enhance laminar mixing over that which would normally occur due to mass diffusion processes alone.

1 Introduction

Laminar flow mixing on the micro-scale is becoming an increasingly important issue with the continuing developments in MEMS-based fluidic systems. The functionality of chip-level devices such as chemical reactors, detectors, and total analytical systems (μTAS) often depends on this capability. [1]. However, there is an inherent difficulty in achieving efficient micro-scale mixing. On the macro-scale, most approaches to mixing rely upon easily-generated flow turbulence and/or mechanical stirrers; however, on the micro-scale this is not feasible. Flow turbulence is highly unlikely because of the characteristically low Reynolds numbers associated with MEMS dimensions and flow rates, although some reports in the literature have suggested the possibility of early transition to turbulence in microchannels. Further, the fabrication and implementation of MEMS mechanical stirrers of sufficient strength and reliability is a challenging task. Therefore, alternative approaches to MEMS mixing systems have been proposed which are based upon laminar flow concepts. A common feature of these laminar mixing systems is a junction where the inlet fluids converge; at this convergence an identifiable interface is formed which is often stable and persists well downstream of the junction. In this paper we shall refer to this interface as a generalized mixing surface, its stability and visual definition providing a measure of the degree of mixing achieved.

Numerous laminar mixing concepts have been proposed in the literature. For a stable interface, using enhanced mass diffusion across the interface is a possible strategy provided the length scale D and diffusivity α are such that the diffusive time scale $\sim D^2/\alpha$ is sufficiently short. This approach has been exploited in the mixing system of Knight *et al.* [2] A more common philosophy in laminar flow mixing is to find ways to actively and/or

*Address all correspondence to this author: darren.hitt@uvm.edu

Copyright © 2010 by ASME

passively disrupt this interface. An example of a passive strategy is that of Yi and Bau [3] who developed a novel microfluidic system of 90° bends which use the internal generation of span-wise Dean vortices at channel bends to self-stir the liquids thereby passively eroding the mixing surface. According to the authors, a limitation of their system is that a large number of bends are required since the vortices are weak and quickly damped at the low Reynolds numbers of their flow. In contrast, Lee *et al.* [4] have developed an active system which produces complex distortions to the interface using a fluctuating source/sink pressure system oriented transverse to the flow direction.

In this study we investigate an alternative, passive mechanism for enhancing laminar mixing: the addition of inert polystyrene microspheres to microchannel flows. It is thought that given the nonlinear velocity profile of developed flow, in addition to a drag force a single particle will experience a variation of pressure across its surface which will induce a spin and translation causing the single particle to travel transverely to the flow in an attempt to find an equilibrium location. This migration is expected to help divert streamlines, with increased effectiveness as the particle concentration increases. The effect of particle interactions are also expected to help aid this process by possibly adding a chaotic nature to particle migration. For these reasons, we will examine the impact of particles of varying size and concentration against a pure mass diffusion process between converging flows of (identical) miscible fluids at a 3-way microchannel 'Y' junction. One of the converging inlet fluids is 'tagged' with soluble fluorescent dye (the other fluid is undyed) and the resulting mass diffusion across their interface is continuously imaged beginning at the junction and ending approximately 140 channel diameters downstream. Using the techniques of fluorescent microscopic imaging and digital image analysis, the degree of mixing is quantified for varying flow states by the measurement of dye concentration (intensity) profiles at downstream locations. It is expected that the addition of particulates to the flow will notably enhance laminar mixing over that which would normally occur due to mass diffusion processes alone.

2 Experimental Methods

2.1 Apparatus

A microfluidic flow system and microchannel translation system has been developed and constructed at the University of Vermont for studying microchannel flows (Figure 1). In this study, a 60° converging 'Y-type' junction has been used with all channels having approximately square cross-sections with a width and depth of 127 μm. The flow rates of each inlet are identical and controlled using programmable syringe pumps (Harvard Apparatus model PHD2000) equipped with 500 $\mu\ell$ Hamilton 'Gas-Tight' syringes. Flow rates were chosen in order to maintain low Reynolds numbers of $O(1)$, based on the mean velocity in the outlet. Typically, this required flow rates to be on the order of 2-30 $\mu\ell$/min (Q_{total}). Only steady flows are considered.

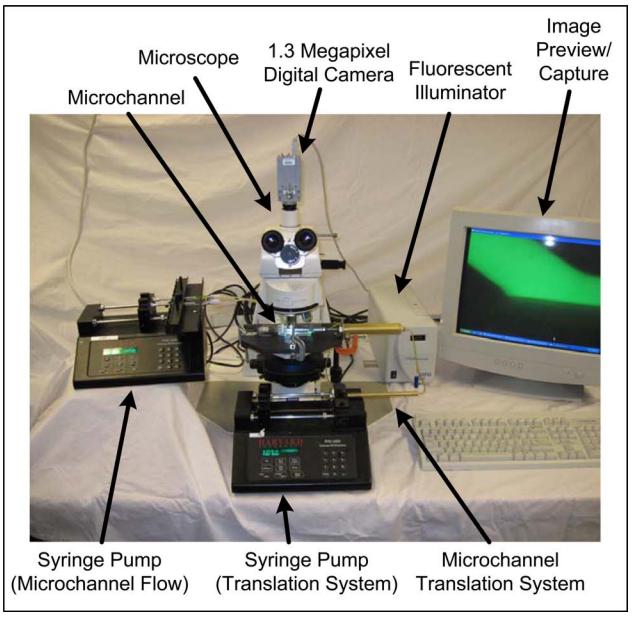

FIGURE 1. Photograph of the experimental apparatus. The experimental setup is comprised of a microscope with top-mounted digital camera, a syringe pump, a fluorescent illuminator, a microchannel translation system with syringe pump, and a monitor displaying images pre- and post-capture.

The inlet fluids are nominally aqueous solutions of sucrose (84% purified, de-ionized water, and 16% sucrose). Particulate suspensions of desired concentration (2.5-10%) are obtained by adding 1 μm and 10 μm diameter polystyrene spheres. The proportions of the aqueous sucrose solution were selected so that the micro-spheres would be neutrally buoyant at room temperature. To permit visualization under fluorescence microscopy, one of the inlet fluids is labeled with a very dilute concentration (0.1%) of FITC/fluoroscein which glows a bright green. A small amount of Tween surfactant is also added to prevent aggregation of the micro-spheres. A sample photographic sequence showing the microchannel's junction with single inlet particle suspensions is shown in Figure 2.

2.2 Microscopic Imaging and Analysis

Experiments have been performed with particles in both a single and double inlet. For the single inlet cases, pure liquid is labeled with FITC whereas the particulate flow is unlabeled; therefore, under fluorescent imaging the particulate fluid is virtually invisible. In the double inlet cases the particles remain invisible even though one of the particulate inlets is labeled with FITC.

Copyright © 2010 by ASME

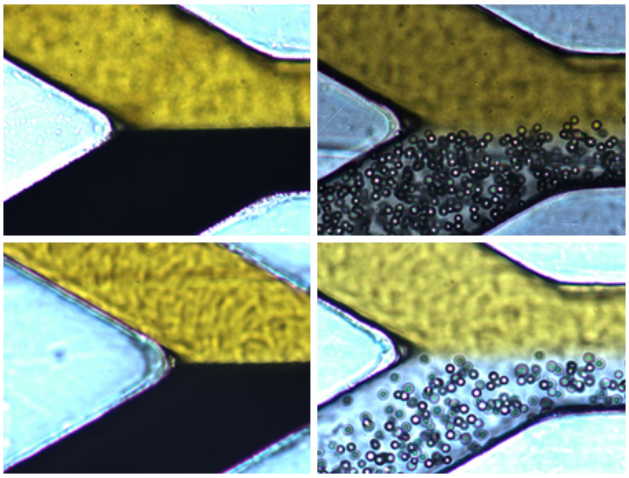

FIGURE 2. A sequence of junction images obtained during experimentation showing differing particle diameters and concentrations; (top left) 1 μm, 5% concentration, (bottom left) 1 μm, 2.5% concentration, (top right) 10 μm, 10 % concentration, and (bottom right) a 10 μm, 5 % concentration. The flow enters from left and leaves to the right, and the same flow rate of 0.25 $\mu\ell$/min is used throughout. The interface is seen as the upper line vertically bounding the particles, as well as the region separating the shaded and clear (unshaded) fluids. For the purpose of particle visualization fluorescent illumination has been been switched off and flow rates have been decreased to permit image capture.

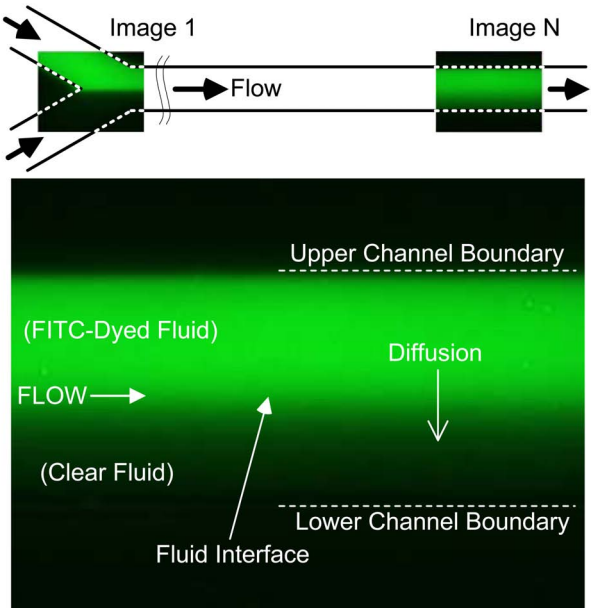

FIGURE 3. (Top) Schematic diagram depicting the microchannel geometry, the image field-of-view (FOV) and the image capture sequence. (Bottom) Sample raw image.

We have found this arrangement an effective means of analyzing the evolution of the separating 'interface' between the flows downstream of the junction. Microscopic imaging is performed using a Zeiss Axioskop2 upright microscope with a 20×/0.3 NA air objective. Digital images of the field flow are recorded using a 1.3 MP PixeLink camera attached to the microscope. Under a prescribed steady flow condition, a sequence of adjacent images are captured in the downstream direction. The first image (Image 1) is captured at the junction of the two converging flows, after which, progressive images ('Image 2' through 'Image N') are captured incrementally downstream of the junction (Figure 3). After capture of the first image, subsequent image locations are determined by precisely translating the microchannel using a hydraulic translation system with better than 99.7% placement accuracy. A slight image overlap is kept so that proper image reconstruction can be verified. With this technique, excellent reconstructablity has been demonstrated and a continuous virtual field-of-view (FOV) extending approximately 140 channel diameters downstream is available for analysis.

All digital images are imported into the MATLAB technical computing software package for further analysis. The input color bitmap is converted to an 8-bit grayscale image, with each pixel having an intensity value bounded between 0 (black) and 255 (white). The analysis of an intensity profile transverse to the channel flow direction then provides a quantitative measure of the interfacial degradation and level of mixing. Specifically, in the absence of mixing a sharp interface exists and one observes a near 'step-change' in intensity as one crosses the interface. As mixing progresses, one observes a smoothing and spreading of the intensity distribution in a manner consistent with a diffusion process. An example of developing intensity profiles is shown in Figure 4 where a particle mixing case is contrasted against a diffusion-driven mixing case. By performing this analytical procedure of comparison for sequentially increasing distance in the downstream direction one can obtain a graphical representation of the diffusion process for the channel as a function of downstream distance and clearly see any enchancement effects.

Experiments have been conducted to examine the convection/diffusion mixing for a range of volumetric flow rates from 1 – 15 $\mu\ell$/min and inlet particle concentrations as high as 10%. Specifically, experiments have been performed for flow rates of 1, 2, 4, 8, 10, 12 and 15 $\mu\ell$/min. For each of these flow rates, a pure-diffusion (reference) set of experiments has been obtained, as well as data sets for particle concentrations of 2.5%, 5% and 10% for 1 μm suspensions and 10 μm suspensions in a single inlet. Lastly, experiments have also been performed for cases of suspensions in both inlets. To qualitatively address the question of how particles in the flow effect mixing, complete sets of experiments have been performed where fluorescence has been switched off (as in Figure 2) so that particle migration can be seen with increasing downstream distance.

Copyright © 2010 by ASME

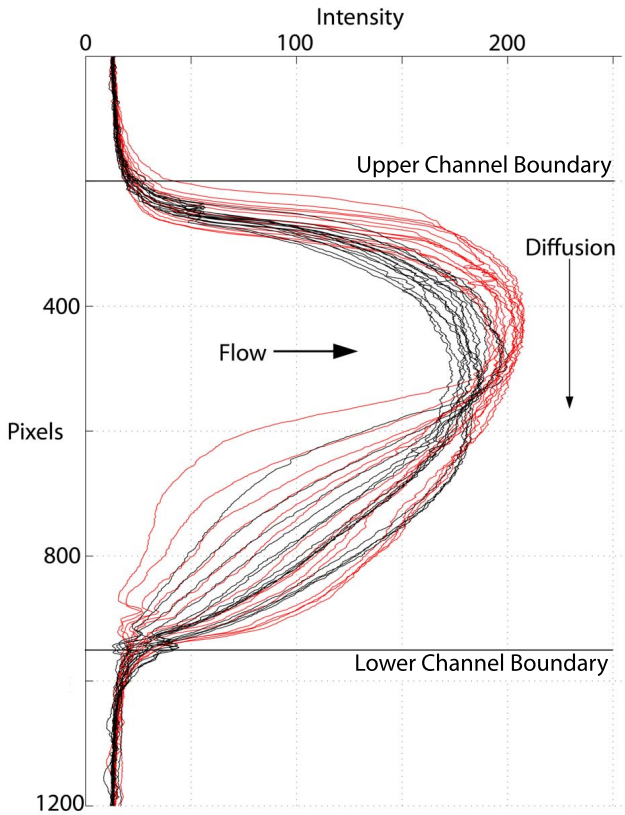

FIGURE 4. Sample intensity profile plot contrasting pure-diffusion (red curves) and particle-enhanced diffusion (black curves) showing collapsing and spreading of curves with progression of downstream distance. Here the flow rate is 2.0 $\mu\ell$/min, the particle size is 1 μm and the particle concentration is 10%.

All concentrations are given by the weight fraction of particles to fluid; therefore for single inlet cases the concentration of particles in the fluid leaving the channel is exactly half that of that being input, while the fraction of particles in the fluid leaving the double inlet cases is exactly equal to that of the input.

3 Experimental Results

In this section we present an overview and summary of the key experimental findings of this study. At the outset, it is important to recognize that the ability to achieve 'complete mixing' within the observational window at the micro-scale is dependent on a combination of factors: the available field of view, the overall flow rate, and the (effective) diffusivity in the transverse direction. As mentioned in §1, an estimate of the time scale for diffusive mixing can be estimated by scaling arguments as[1]

$$t_d \sim \frac{D^2}{\alpha} \tag{1}$$

where D is the channel width and α is the effective mass diffusivity. The associated mixing length L can then be estimated based on the mean flow velocity U as $L \sim U\, t_d$ with the result

$$\frac{L}{D} \sim \frac{UD}{\alpha} = Pe \tag{2}$$

where Pe is the Péclet number based on the mass diffusivity. The number of channel diameters required for mixing thus scales proportionally with the Péclet number. For a mass diffusion problem, even on the micro-scale, the value of the Péclet number is not necessarily small. Experimentally, we are limited by the field of view to a maximum downstream distance of *approximately 140 diameters*. For flow conditions with $Pe > 140$ one cannot expect to observe complete mixing; rather, one will observe only an approach to complete mixing and the degree of which will depend on the magnitude of Pe. Therefore, with the exception of very low Pe cases, it is often more relevant to discuss empirical 'mixing rates' rather than the final mixing length itself.

A typical set of experimental image data appears in Figure 5-6. In Figure 5, a collection of raw images representing approximately one-fourth (35 channel diameters) of the test section is shown. From this sequence, a single composite image can be reconstructed (Figure 6). It is important to note that these last two figures represent only a downstream distance of 35 channel diameters; this has been done for purposes of clarity. The actual image sets used in quantitative analyses extend nearly 4× further downstream.

3.1 Particle Migration

Before proceeding to the quantitative mixing results, it is worthwhile to provide direct image evidence of the particle migration across the channel width. Referring to Figure 2, one can see how particles in converging flows at the junction are diverted and initially follow streamlines, as is consistent with the low Stokes numbers of this flow. Further downstream, however, there is clear evidence of particle migration transverse to the flow direction (Figure 7). It is interesting to note that the while both visualizations show evidence of hydrodynamically-driven particle migration, the smaller 1 μm particles appear to move together in a broadening 'band' suggesting that particle interactions are more dominant than for cases of fewer, but larger particles. This visual evidence suggests, intuitively, that cases

[1] We do not consider the effects of Taylor dispersion and the associated increase in effective mass diffusivity.

Copyright © 2010 by ASME

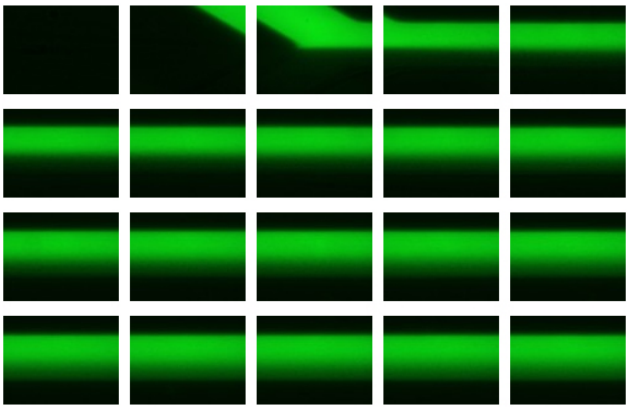

FIGURE 5. Sample color (8-bit RGB) montage of 21 raw images collected for a non-particle (reference) experiment with a flow rate of 1.0 $\mu\ell$/min. For this low flow rate, diffusive mixing can be seen in relatively short distances.

FIGURE 6. Sample (8-bit) grayscale composite image built from the raw images seen in Figure 5. The smoothness and continuousness of these composite images allows for excellent visualization and analysis of each experiment.

with larger and more dispersed particles might be more effective at inducing mixing due to their greater mobility.

3.2 Mixing Metrics

To establish a metric for the mixing progression in the downstream direction, we adopt a measure proposed by Liu *et al.* [5]-[6] and introduce a local mixing coefficient C defined over an image region $\mathscr{A}$ containing N pixels

$$C = \frac{\sqrt{\frac{1}{N}\sum_{i=1}^{N}(I_i - I_{mean})^2}}{2^n - 1} \tag{3}$$

Here I_i is the intensity value for each pixel, I_{mean} is the mean intensity value over the selected region, and n is the image resolution in bits (8-bit in our case). Essentially, this formula represents a statistical intensity variance (second moment) over the area of interest normalized by the number of gray levels $(2^n - 1)$. In the limit of $C \to 0$ this metric thus indicates perfect mixing; in practice, this cannot be realized due to experimental noise as well as non-perfect mixing and one expects instead the metric to asymptote to some finite, presumably small value. It is evident that this metric is also dependent on the degree of 'localization'

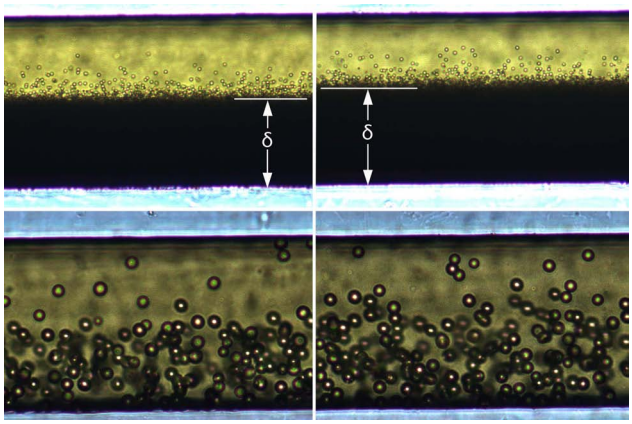

FIGURE 7. Non-fluorescent images of particle experiments with 1 μm, 5% particle concentration taken at about 70 channel diameters (top left) and 140 channel diameters (top right), and 10 μm, 10% particle concentration taken at about 70 channel diameters (bottom left) and 140 channel diameters (bottom right). The flow rate used throughout is 0.25 $\mu\ell$/min so that particles can be imaged by the camera. Note the broadening of the particle 'band' height δ.

represented by the region $\mathscr{A}$ being examined. Ideally one could select a single column of image data across the channel section to serve as the area and thus obtain a highly localized value. However, this must be balanced against the desirable averaging out of noise in the data set by expanding the region $\mathscr{A}$. In our study we have found the noise level sufficiently low that a single column of data can in fact be used and the area $\mathscr{A}$ is 1×650 pixels, with the latter dimension being the channel width.

In addition to the normalized intensity variance C, another parameter that can be computed is the normalized third-moment or 'skewness' S of the intensity distribution. The value of computing this quantity is to assess the degree to which the statistical variations are symmetrically distributed about the mean intensity. One expects that the combination of C and S tending toward zero provides a stronger statement of complete mixing.

Illustrations of the mixing coefficient evolution in the downstream direction are shown in Figure 8 for particle sizes of 1 and 10 μm at concentrations of 2.5% and 5% at the lowest flow rate of 1.0 $\mu\ell$/min. The particle free case is also shown for reference. A first observation is that there is a finite amount of scatter present in all data sets, and it seems more pronounced with distance downstream. Accounting for the scatter, all plots demonstrate the expected decay in the metric C, however it is evident that complete mixing has not been achieved even for this lowest flow rate under consideration. Also evident is an impact of the particulate presence. As the particle concentration goes from 0% to 2.5% decay rate is observed to increase; however, further increase in particle concentration to a level of 5% causes the decay rate to diminish. At still larger concentrations of 10% (not

Copyright © 2010 by ASME

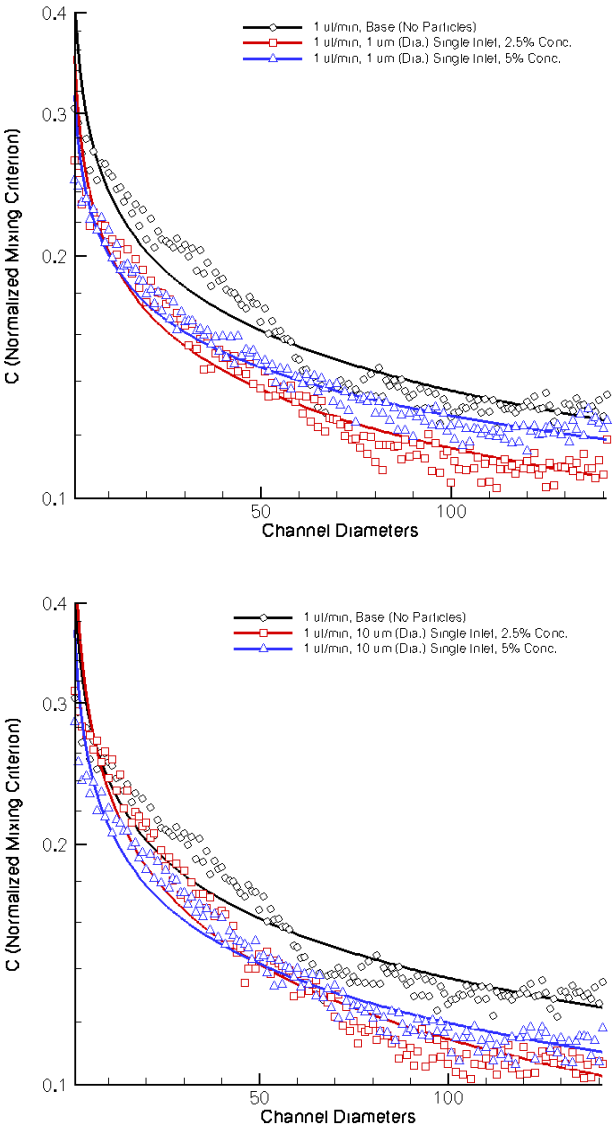

FIGURE 8. Illustrations of the mixing coefficient evolution as a function of downstream position. Shown in these figures are cases of 1 μm particles (top) and 10 μm particles (bottom) at different concentrations and for a flow rate of 1.0 $\mu\ell$/min. Also shown for reference is the particle-free case. A semi-log scale is shown for clarity.

shown in the figure) the mixing results are very similar to those at 5%. This trend is common to both cases of small and large particles. It is also noteworthy that, for a fixed concentration, the decay rate appears to be relatively higher for the larger particles as compared to the smaller particles as previously suggested based on Figure 7.

In order to extract a single, summarizing mixing statistic for each experimental case, the mixing curve evolution is fit to an empirical power law of the form

$$C(x) = e^A x^k \tag{4}$$

using a least-squares approach where x is the downstream location, A is a constant and k is the empirical decay rate. This decay rate k can be interpreted as a relative mixing rate for a given flow condition. The associated curve fits also appear with the plots of Figure 8 which demonstrate reasonable overall agreement with the data trends. However, the match only approximates the data because the empirical power law does not accurately capture the mixing behavior over the entire downstream region. Nonetheless, this power law exponent does represent a useful statistic to compare different cases.

Shown in Figure 9 are plots of the power law exponent (i.e., mixing rate) as a function of overall flow rate for different particle sizes and concentrations. It is clear that, regardless of particle conditions, that the mixing rate diminishes – k decreases in magnitude – as the flow rate is increased. This is to be expected from Eq. (2) since higher flow rates correspond to higher Péclet numbers. The exact interpretation of the particle impact is less clear. At the higher flow rates, there is generally little distinction between particle conditions considering the experimental uncertainty and the quality of the power law curve fit. A notable exception to this is for the smaller 1 μm particle case at a concentration of 10% which appears to promote mixing over a range of flow rates. Interestingly, for suspensions of larger 10 μm particles, there is little variation between particle and particle-free cases over the entire flow range with the exception of the 2.5% concentration: this condition appears to yield uniformly enhanced mixing rates. In summary, the power law exponent data, on the whole, do not seem to indicate any clear or profound impact of the particulate presence in the flow.

Lastly, we introduce one additional metric in an effort to quantify the extent of the mixing that is observable within the experimental domain. Following once again the methods of [6] we define a 'mixing efficiency' η according to

$$\eta = \frac{C_{inlet} - C_{outlet}}{C_{inlet}} \tag{5}$$

where C is the mixing coefficient defined in Eq. (3); this normalized metric thus ranges from zero (unmixed) to unity or 100%(perfectly mixed). Plots of the efficiency parameter for different particle sizes and concentrations appear in Figures 10-11 for two different levels of flow rate. The disparity in mixing efficiency between the two cases is quite striking, and it is evident that at the flow rate of 8 $\mu\ell$/min there is only a modest level of mixing achieved within the experimental domain. In contrast, for the lowest flow rate of 1 $\mu\ell$/min all curves asymptote towards a steady level of mixing efficiency far downstream. It is

Copyright © 2010 by ASME

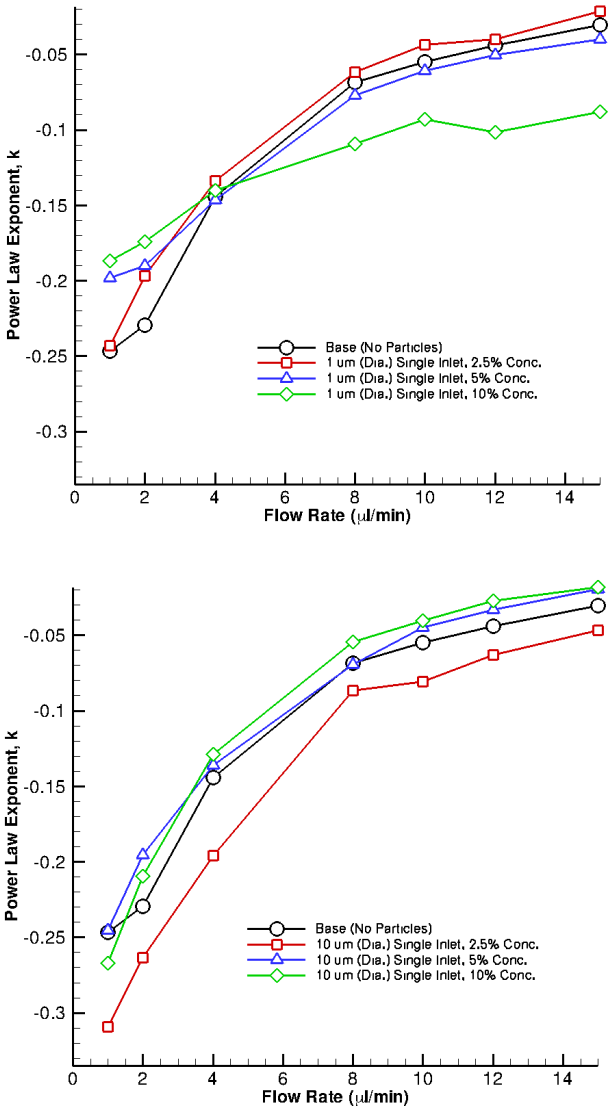

FIGURE 9. Plots of the power law exponent determined from curve fits of the mixing coefficient data under different flow rates and particle conditions.

notable that the mixing efficiency does not tend toward a value of unity (or 100%) since, as seen previously, the mixing coefficient C does not tend to zero but rather a finite, small constant. For the smaller particles at 2.5% concentration, the efficiency curve is essentially identical with the particle free case. As the particle concentration is increased to 5% and 10%, there is separation from the other data and these curves *approach their asymptotic value somewhat sooner* – although the difference between these two concentrations is minimal. For the case of larger particles, the asymptotic efficiency values are observed to be larger overall than for smaller particles, however the actual variation in this value is not substantial. Still, the mixing efficiency is higher for all cases with particles over the particle-free case; however, there is not a direct correlation with concentration. Rather, it seems that it may be that the introduction of particles increases efficiency but only up to a point after which the efficiency again diminishes. In summary here, while it can be stated that mixing is likely 'complete' in the low flow rate cases given the asymptotic curve behavior, the precise impact of the particles is not immediately obvious.

4 Discussion

The experimental findings suggest that the role of particles in the diffusive mixing process may be rather subtle, at least for the hydrodynamic conditions examined in this study. Only minor variations were observed in the metrics employed to characterize the mixing process. Two possible explanations present themselves. First, it is possible that under these hydrodynamic conditions the particles are essentially passive components with little impact on the diffusive mixing. Second, it may be that the metrics used to characterize the mixing do not properly account for the particle impact on the actual imaging data. These metrics were previously utilized for the study of microchannel mixing between single phase fluids. In this work is reasonable to posit that the optical characteristics of the particles affect the florescent imaging data. These particles are relatively large in comparison to the microchannel diameter and have a finite reflectivity, being semi-transparent. As a result, even for a perfectly mixed fluid with a uniform distribution of particles, one might expect that the intensity variance would be nonzero. This can be understood by re-examining Figure 7. In considering the mixing efficiency plots it follows that all cases essentially begin with the same inlet mixing coefficient C; however, the outlet value for even a fully mixed case may well depend upon the particle distribution, size, and optical characteristics because of the nonuniformity in intensity. Then one would not expect fully mixed curves to asymptote to the same mixing efficiency. In short, the quantity of interest in the mixing efficiency plots may not be the asymptotic value but rather the derivative of these curves which could represent the rate of mixing with downstream distance.

Yet another factor that must be considered here is the three-dimensional nature of the actual flow compared to the two-dimensional imaging being employed. The two-dimensional image data represents an intensity based on the fluorescent emissions integrated through the depth of the channel. This inherently introduces a degree of averaging into the measurement technique that could, in some way, contribute to masking some of the variations between different flow conditions if they are as subtle as they appear.

Of the particle-based variations that have been observed, there does not seem to be a simple correlation between size, con-

Copyright © 2010 by ASME

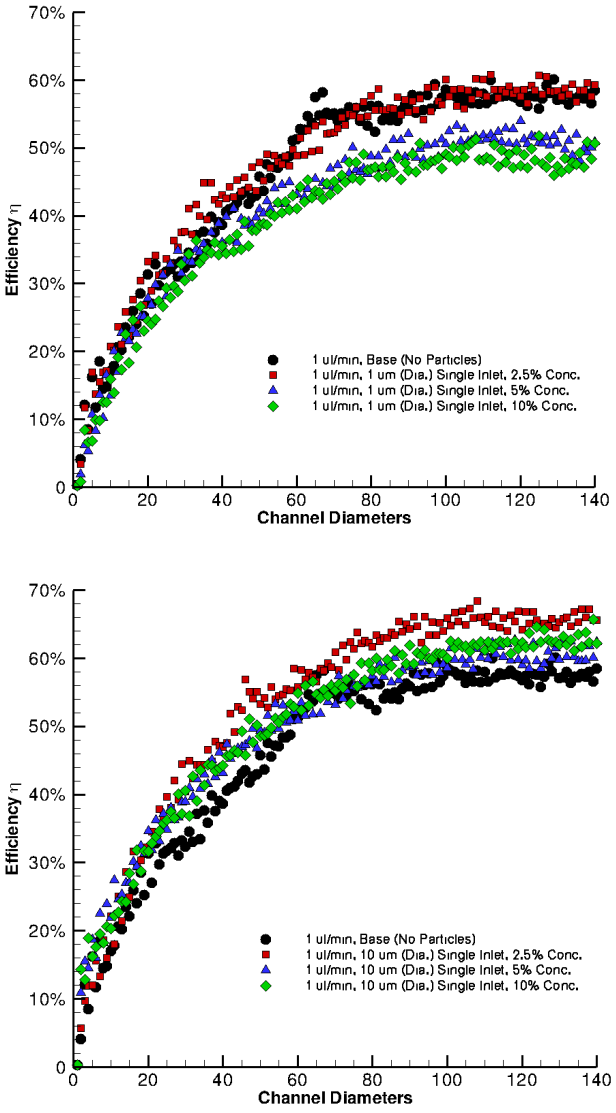

FIGURE 10. Plots of the mixing efficiency for different particle sizes and concentrations at a flow rate of 1 $\mu\ell$/min: (top) 1 μm particles; (bottom) 10 μm particles. The asymptotic approach to a final efficiency level is apparent.

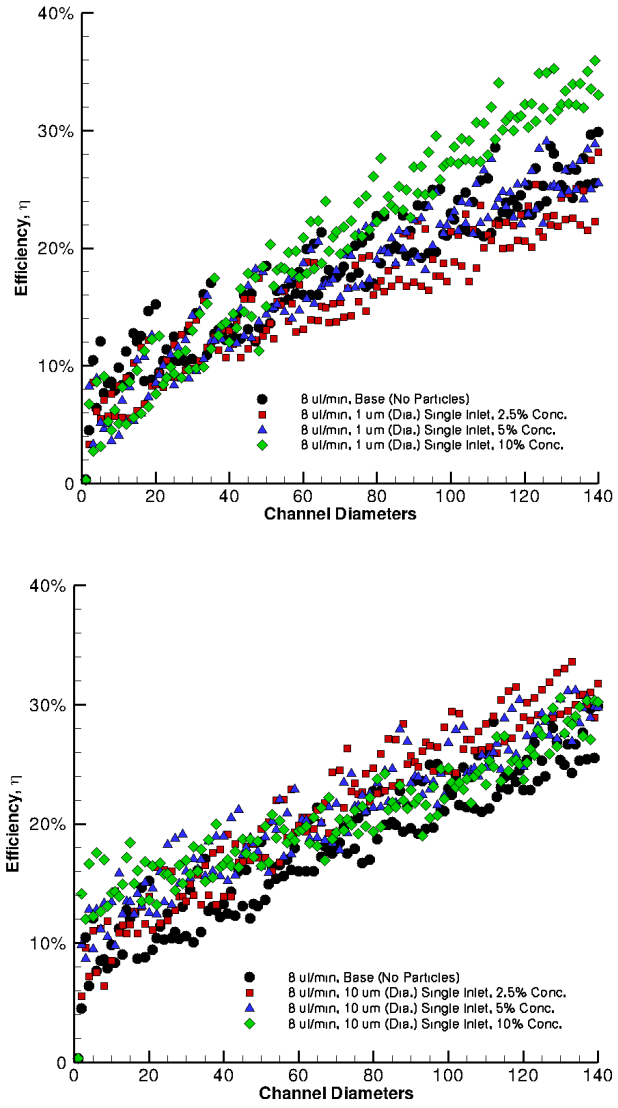

FIGURE 11. Plots of the mixing efficiency for different particle sizes and concentrations at a flow rate of 8 $\mu\ell$/min: (top) 1 μm particles; (bottom) 10 μm particles. No asymptotic behavior is observed.

centration and mixing efficiency. Rather, the data suggests that there are parametric combination(s) that produce the greatest enhancement on mixing. This is likely connected to the 'mobility' of the individual particles which, in turn, depends in a complicated way on the hydrodynamic shear forces as well as inter-particle interactions. As the suspensions used in this work are not dilute, these interactions may be quite complicated and could be a possible explanation for the indeterminate findings in this study.

5 Conclusions

The goal of this experimental study has been to delineate the impact of rigid particles on diffusive mixing in a microchannel. The microfluidics literature, while robust with studies of microchannel mixing schemes with multiple fluids, is nonetheless lacking in mixing studies involving particle suspensions. The microchannel setting is especially challenging and unique because the particles themselves may be substantial in size in relation to the channel diameter; this is in sharp contrast to traditional macro scale studies involving suspensions. We have examined

Copyright © 2010 by ASME

particle concentrations up to 10% and have utilized particles that are approximately 1% and 10% the size of the channel diameter. The findings of this work are somewhat inconclusive in the sense that no substantial impact on the mixing efficiency has been observed for a variety of particulate flow conditions. Consequently, we must conclude that the utilization of particles as a passive scheme for enhancing diffusive mixing in microchannels offers little if any advantages over existing techniques. Another perspective is that, for flows involving particular conditions similar to this study, the simplifying assumption that the suspension may be regarded as a continuous fluid may be safely invoked for calculations or simulations of diffusive mixing.

ACKNOWLEDGMENT

This work has been partially supported by NASA under cooperative agreements NCC5-581 and NNG05GH16H.

REFERENCES

[1] Stone, H.A., Strook, A.D., and Adjari, A., 2004, "Engineering Flows in Small Devices: Microfluidics Toward Lab-on-a-Chip," Annual Review of Fluid Mechanics, **36**, pp 381-411.

[2] Knight, J.B., Vishwanath, A., Brody, J.P., and R.H. Austin., 1998, "Hydrodynamic Focusing on a Silicon Chip: Mixing Nanoliters in Microseconds," Phys. Rev. Lett., **80**. pp 3863-3866.

[3] M. Yi and Bau H.H.. "The Kinematics of Bend-Induced Stirring in Micro-Conduits." In Microelectromechanical Systems (MEMS) 2000, Proceedings of the 2000 ASME International Mechanical Engineering Congress & Exposition, pp 489–486. American Society of Mechanical Engineers, 2000.

[4] Lee, Y.-K., Tabeling, P., Shih, C., and Ho, C.-M., "Characterization of a MEMS-Fabricated Mixing Device." In Microelectromechanical Systems (MEMS) 2000, volume Proceedings of the 2000 ASME International Mechanical Engineering Congress & Exposition, pp 505-511. American Society of Mechanical Engineers, 2000.

[5] Liu, R.H., Stremler, M.A., Sharp, K.V., Olsen, M.G., Santiago, J.G., Adrian, R.J., Aref, H., and Beebe, D.J., 2000, "Passive Mixing in a Three Dimensional Serpentine Microchannel." J. MEMS 9, 190.

[6] Liu,Y.Z., Byoung, J.K., Hyung, J.S., 2004, "Two-Fluid Mixing in a Microchannel." International Journal of Heat and Fluid Flow, **25**, pp 986-995.

Copyright © 2010 by ASME